RSC Advances

ROYAL SOCIETY OF CHEMISTRY

www.rsc.org/advances

RSC Advances

RSCPublishing

ARTICLE

Method to Construct Perfect 3D Polymer/Graphene Oxide Core-Shell Microspheres: Electrostatic Self-Assembly

Cite this: DOI: 10.1039/xoxxoooooox

Received ooth January 2012,
Accepted ooth January 2012

DOI: 10.1039/xoxxoooooox

www.rsc.org/

Ying Li,[a] Yu Xu,[a] Tao Zhou,[a,*] Aiming Zhang,[a] and Jianjun Bao[a,b,*]

In this study, a method to construct perfect three-dimensional (3D) polymer/graphene oxide (GO) core-shell microspheres was proposed using the electrostatic self-assembly. 2D GO nanosheets were successfully wrapped onto polymer microsphere to form a perfect 3D core-shell structure with a uniform shell thickness under the action of the electrostatic attraction force. The GO nanosheets with 1.5-2 nm thickness and the area over 2×1 μm^2 were firstly prepared from graphite, and then the cationic polystyrene (PS) microspheres with 0.246% and 0.715% surface concentration of $-N(CH_3)_3^+$ were successfully synthesized. After that, PS/GO core-shell microspheres were constructed between GO nanosheets and the cationic PS microspheres. It was found that different cationic PS microspheres leaded to different assembly speed. The SEM and TEM images of rippled silk waves on the surface of PS/GO core-shell microspheres not only indicated the perfect polymer/GO core-shell structure, but also presented a strong binding between two materials. It was also revealed that the thickness of the shell of PS/GO core-shell microspheres was under good control, and the thickness of the shell from different cationic PS microspheres was 9-13 nm and 80-100 nm, respectively. The method proposed here has proved to be a valuable tool for the assembly of 3D microstructures from polymers and graphene oxide (or graphene).

1. Introduction

Graphene,[1] a single carbon sheet with 2D honeycomb crystal lattice structure made up of hexagonal carbon rings, is supposed to be the most potential nano materials with excellent conductivity,[2-4] mechanical property,[5] thermal conductivity[6] and electrochemical property[7]. Thus, its potential applications have been widely developed in the fields of polymer composites,[8, 9] biomedical sciences,[10] sensors,[11] batteries,[12] supercapacitors,[13] and photocatalysis[14]. Graphene has been used as a perfect 2D material in most of the recent applications. Low-dimensional materials such as 2D graphene can achieve good strength in part because of the lack of surface defects that often initiate fracture in 3D materials,[15] so it is always necessary for graphene or graphene oxide to construct three-dimensional (3D) macrostructures for the suitable use of the real-life devices. Therefore, developing a method to transform the nanosheets into three-dimensional macrostructures with a uniform thickness is of a great significance.

The well-established strategies such as spin-coating,[16] filtration,[17, 18] layer-by-layer (LbL) assembly,[19, 20] and Langmuir–Blodgettry[21, 22] can transform the nanosheets into thin or ultra-thin film structures. On the contrary, constructing a thicker structure has a great difficulty. As everyone knows, because of the high specific surface area, the original 2D lamellar structure is easily distorted and aggregated into other uncontrolled shapes, resulting in a sharp decline in performance. Therefore, an important issue is how to construct a 3D macrostructure with a uniform thickness and avoiding agglomeration during the process. Several studies have investigated 3D nanostructures of graphene in recent reports,[23-31] of which, the most common way was the hydrothermal method to graphene oxide (GO) suspension. Xie[32] reported the preparation of PS particles using GO nanosheets as the stabilizer, and an intricate method which was sensitive to the initiator and the slight change of pH was provided. Yang[33] studied a self-assembly method to prepare a PMMA/graphene composite, and it was reported that PMMA/GO complex particles were formed due to the interaction between GO nanosheets and PMMA particles. Huang et al.[34] introduced a method of surface modification to form an almost perfect SiO_2/GO hybrids. Li et al.[35] reported a facile method to fabricate polystyrene/graphene core-shell microspheres through

electrostatic interaction. The polystyrene microspheres were prepared by emulsion homopolymerization using 2,2'-Azobis(2-methylpropionamidine) dihydrochloride (AIBA) as a cationic initiator. In their work, the cationic groups in PS microspheres were the residues of AIBA (initiator residues). In general, the amount of the initiator used in emulsion polymerization is very low. The positive charge is derived from positively charged cationic groups. Thus, in their study, the positive charge on the surface of cationic PS microspheres was very small. This will lead to a thin shell thickness of core-shell microspheres, and the shell thickness certainly cannot be controlled.

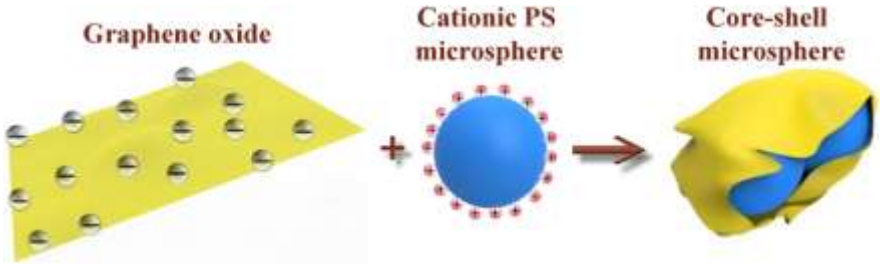

Fig. 1 Sketch of the process of the electrostatic self-assembly

Herein, a perfect 3D polymer/graphene oxide (GO) core-shell microsphere is fabricated via the electrostatic self-assembly. Considering that the graphene has no functional groups on its surface, a well-dispersed graphene oxide becomes a best bridge to construct it. The availability of oxygen-containing functional groups on the basal plane and edge allows GO sheets to interact with each other or to disperse in a variety of organic and inorganic materials to form a desired structure. In this work, GO nanosheets possessing negative charges overlaid and attach tightly around cationic PS microspheres by electrostatic attraction. Different from other 3D graphene or graphene oxide microstructures, the thickness of this shell structure is relatively uniform and truly controllable. The whole process of the electrostatic self-assembly is totally spontaneous, and the formed core-shell structure can withstand intense agitation and ultrasonic treatment without being destroyed. The sketch of the electrostatic self-assembly is shown in **Figure 1**. Moreover, the bonding force of the assembly is very strong and can be utilized in various applications, such as to create free-standing architectures with tailored shapes or to transform 2D graphene oxide nanosheets into various 3D structures. With such serviceable characteristic, we believe that this technique is probably a valuable tool for the assembly of nanostructure or nanomaterial.

2. Experimental

2.1. Materials

Graphene oxide was prepared via modified Hummers method[36] using crystalline flake graphite as the raw material. Crystalline flake graphite was bought from Qingdao Tianheda Graphite Co., Ltd. Styrene was distillated under vacuum to remove inhibitors. Azobisisobutyronitrile (AIBN) was refined before use by recrystallization in methanol. Styrene, AIBN, DMC, polyvinyl pyrrolidone (K30), and ethanol were all analytical grade and used as merchandise.

2.2. Preparation of polymer/graphene oxide core-shell microspheres

Preparation of the polymer/GO core-shell microspheres can be divided into two steps:

1) Copolymerization with a kind of cationic monomer to get a positively charged polystyrene (PS) microsphere;

2) The electrostatic assembly of the negative exfoliated GO sheets with the cationic PS microspheres.

Cationic PS microspheres were prepared using the dispersed emulsion polymerization. 0.8 g polyvinyl pyrrolidone was added into a three-necked flask containing 40 mL deionized water and 30 mL ethanol. A water bath was used at 70 °C together with the mechanical stirring at a speed of 300 rpm under nitrogen atmosphere. Half an hour later, the styrene of 2 g and AIBN of 0.2 g were added into the mixture. After the mixture turning into a little white, the solution of 0.2 g AIBN, 6 g styrene, and DMC (2 wt %, 10 wt % of styrene dissolved in 30 mL ethanol) was added drop by drop. This adding process was ended at 2 hours later, and then the system was refluxed at 70 °C for another 3 h under nitrogen atmosphere. The solid contents of the emulsions were 8.33 wt%, 8.34 wt%, respectively. The emulsions with 2 wt% and 10 wt% DMC were named as cationic PS 002 and cationic PS 010 in the present study. A pure polystyrene emulsion was also prepared according to the above procedure, only without DMC.

PS/GO core-shell microspheres were prepared by simply mixing cationic PS microspheres emulsion with GO aqueous solution. The aqueous solution of GO (0.3 wt %) was prepared by high-power ultrasonication for 30 min and high-speed (>8000 rad/min) centrifugation three times. The 5 mL resultant diluted GO solution (diluted 100 times) was added dropwise into the 5 mL diluted emulsion (diluted 100 times) under agitation. After the stirring was stopped, PS/GO core-shell microspheres were precipitated at the bottom of the beaker, leaving the upper nearly transparent aqueous solution.

PS/GO core-shell microspheres were put at room temperature for completely aggregation.

2.3. Characterizations

2.3.1. AFM

Atomic force microscope (AFM) micrograph of GO was obtained on a Multimode Autoprobe CP/MT Scanning Probe Microscope (Veeco Instruments, Woodbury, NY). The GO solution of 0.01 mg/mL was dropped in nude mica surface, dried in the dryer at room temperature until the test. The tapping mode was used, and the scan rate was 1.0 Hz.

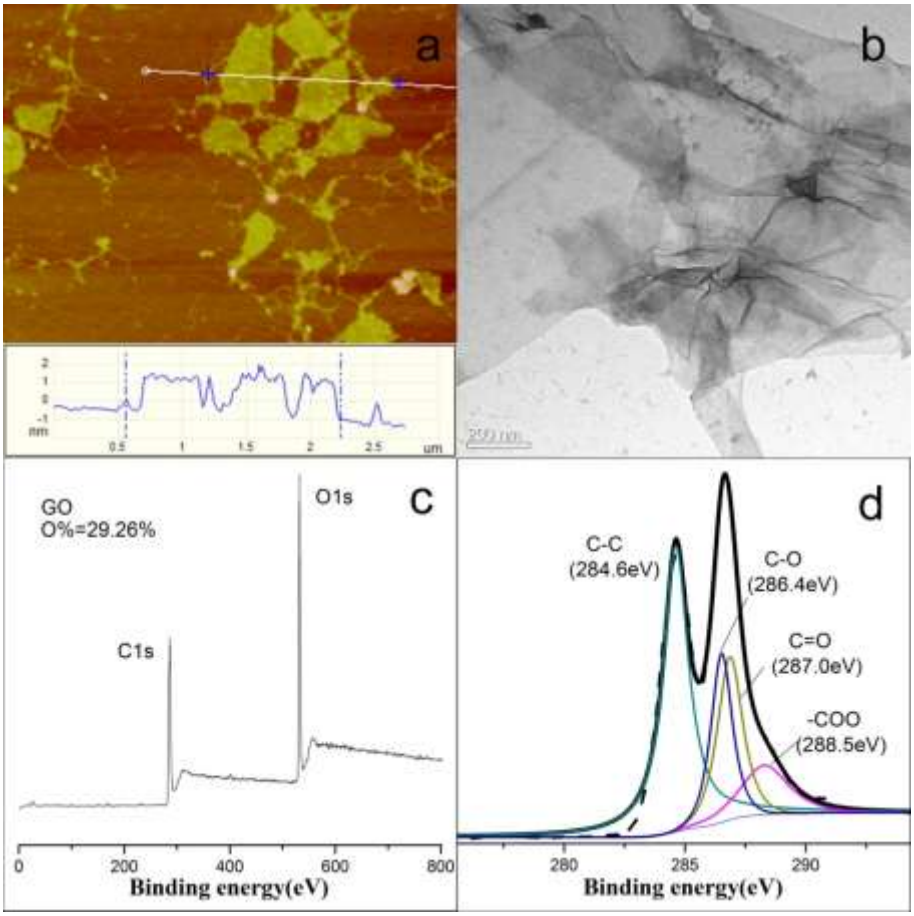

Fig. 2 Characterizations of graphene oxide. **(a)** AFM height image of graphene oxide nanosheets; **(b)** TEM image of graphene oxide nanosheets; **(c)** XPS spectrum; **(d)** C1s XPS spectrum of GO.

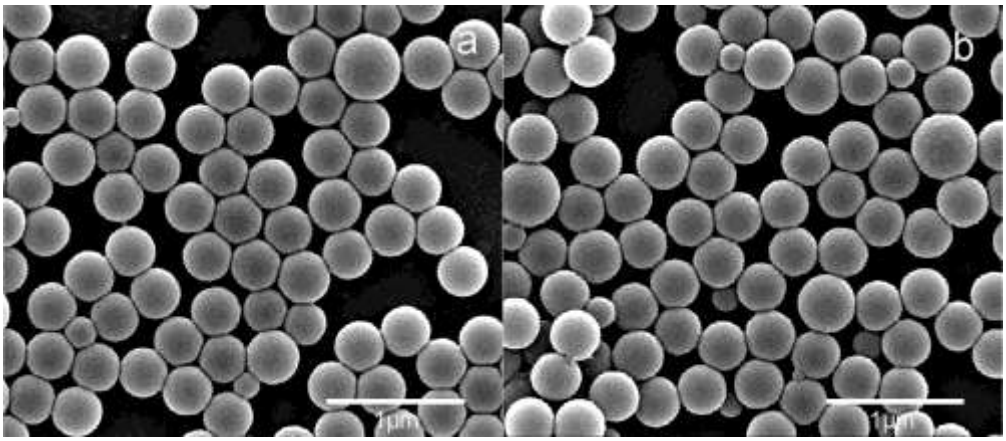

Fig. 3 SEM images of cationic PS microspheres. **(a)** cationic PS 002 microspheres; **(b)** cationic PS 010 microspheres. Please see section 2.2 for the meaning of 002 and 010.

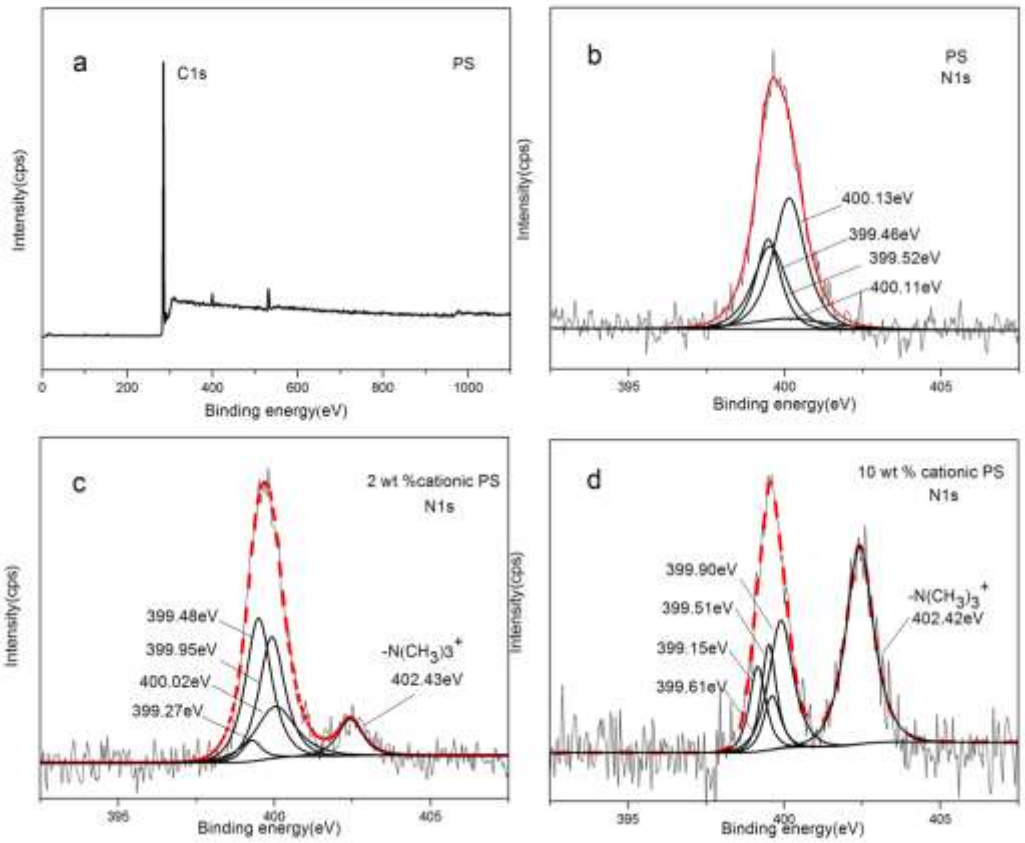

Fig. 4 XPS spectra. **(a)** powders of pure PS microspheres ; **(b)** N1s spectra of pure PS microspheres; **(c)** N1s spectra of cationic PS 002 microspheres; **(d)** N1s spectra of cationic PS 010 microspheres.

2.3.2. SEM and TEM

Scanning electron microscopy (SEM, Hitachi Limited S-3400, Japan) with an acceleration voltage of 10 kV was applied to analyzing morphology of cationic PS microspheres and PS/GO core-shell microspheres. The samples were diluted in a certain concentration and dried on the coverslip in the dryer over night. TEM was characterized on a Tecnai G^2 F20 microscope. All samples were prepared at room temperature by using a droplet of the diluted water of the sample on a copper grid and make it dried in the air.

2.3.3. XPS

The powders of GO, PS microspheres, and cationic PS microspheres were pulverized and detected by X-ray photoelectron spectroscopy (XPS). Oxygen content on GO and element N content of the polymer surface can be obtained by calculation. X-ray photoelectron spectra were recorded on a Kratos Axis Ultra-DLD system with Al Kα, 1000 meV, and 150W.

2.3.4. Zeta potential

The zeta potential of cationic PS emulsion and GO were determined by dynamic light scattering (DLS) using a Malvern Zetasizer Nano-ZS with a laser of 532 nm wavelength at 25 °C. The emulsions and GO dispersion were diluted 100 times with deionized water before the test. All the samples were pH neutral in tests.

2.3.5. Particle size analysis

Particle size analysis was conducted on laser particle size analyzer Mastersizer 2000. The samples of cationic microspheres emulsions were diluted with water for testing.

2.3.6. XRD

X-ray diffraction was measured using X' Pert PRO diffractometer (PANalytical, Holland) with Cu radiation of 40 kV and 35 mA. Samples were all powders and the scanning speed and step size were 0.2 °/min and 0.03°, respectively.

3. Results and discussion

3.1. Graphene oxide

AFM image, TEM image, and XPS spectra of GO nanosheets are shown in **Figure 2**. The sample of GO exfoliated by ultrasonic treatment was diluted by water for AFM and TEM testing. In **Figure 2**, it can be measured that the area of nanosheets is over 2×1 μm^2, and the AFM height image shows that the thickness of nanosheets is 1.5-2 nm, demonstrating the complete of the exfoliation of ultrasonic treatment. In general, a pure graphene has a thickness of 0.34

nm, and a graphene oxide possesses a thicker size due to epoxy and hydroxyl groups randomly distributing on the basal plane and several layers stacking together. **Figure 2(c)** and **Figure 2(d)** illustrate the XPS spectra of GO. The oxygen content of GO is calculated as 29.26 wt%, indicating a high degree of oxidation. The C1s XPS spectrum of GO can be fitted into four peaks in the region of 284.6-288.5 eV, which represents the existence of four different carbon valence bonds.[37] From the C1s XPS spectrum of GO, it is proved the generation of hydroxyl, epoxide, and carboxyl groups after oxidation. These groups are hydrophilic, and therefore, GO can be easily made into an aqueous suspension. The zeta potential of GO is -40.3 mV, which is in accordance with the reported values.[38] The results above indicate the successful preparation of the GO nanosheets from graphite.

3.2. Cationic polymer microspheres

In this study, the cationic PS microspheres are successfully gained. **Figure 3** shows the SEM images of 002 and 010 cationic PS microspheres. The zeta potentials of 002 cationic PS microspheres and 010 cationic PS microspheres are +37.1 mV and +70.3 mV, respectively. Similar results were reported in the literature.[39, 40] Reversal potentials enable strong electrostatic interaction between cationic PS microspheres and GO nanosheets. The average particle size of 002 cationic PS microspheres is D(0.5)=0.351 μm, and that of 010 cationic PS microspheres is D(0.5)=0.336 μm. The D(0.5) is the particle size from a volume fraction of 50%, it can be regard as the volume average particle size.

XPS was measured to prove the existence of the cationic group, which plays an important role during the process of self-assembly. Compared with **Figure 4(b)**, an obviously new peak located at 402.42 eV is observed in **Figure 4(c)** and **Figure 4(d)**, indicating the generation of the cationic group.[41] The other states of N1s from PVP and AIBN exist in the binding energy of 399-401 eV.[42] Here, an equation to determine the surface concentration of an element from XPS is given below:

$$C_x=(A_x/S_x)/(\sum A_i/S_i)$$

where C_x is the surface concentration of desired element, and A_x is the peak area of desired element. S_x is the sensitivity factor.

The actual concentration of $-N(CH_3)_3^+$ was calculated according to the equation above. The surface charge density depends on the concentration of $-N(CH_3)_3^+$, therefore, the surface charge density can be calculated from the $-N(CH_3)_3^+$ group. Then, the issue becomes to calculate the state of $-N(CH_3)_3^+$ among all the N-containing groups. For the cationic PS 002 microspheres, the measured surface concentration of N element in $-N(CH_3)_3^+$ is 0.246%. However, the theoretical concentration of N element in $-N(CH_3)_3^+$ is 0.106%. The actual concentration is more than twice of theoretical value. We think these results can be interpreted from the strong hydrophilic of cationic monomer. The hydrophilic $-N(CH_3)_3^+$ will certainly migrate toward the surface of the cationic PS microspheres in solution, resulting in the enhancement of the actual surface concentration of N element in $-N(CH_3)_3^+$. Similarly, the cationic PS 010 microspheres gain a surface concentration of N element in $-N(CH_3)_3^+$ at 0.715%, which is also higher than the theoretical value (0.506%). The migration of $-N(CH_3)_3^+$ to the surface of the cationic PS microspheres is a good phenomenon for our work, because the surface concentration of $-N(CH_3)_3^+$ is proportional to the surface charge density, which plays an important rule on electrostatic self-assembly.

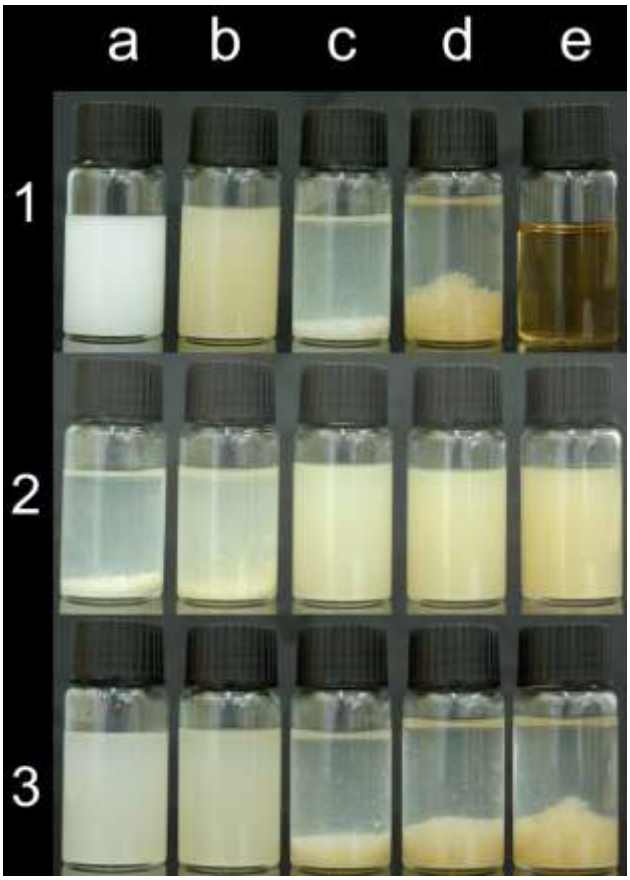

Fig. 5 Digital images of electrostatic self-assembly after 240 min. In the first row, (1-a) 3 wt % cationic PS emulsion; (1-b) 3 wt % pure PS emulsion mixed with 3 wt % GO aqueous suspension, which produces no sediment; (1-c) 3 wt% cationic PS 002 mixed with 1 wt% GO; (1-d) 3 wt% cationic PS 010 mixed with 5 wt% GO; (1-e) 3 wt% GO aqueous suspension. In the second row, 2-a, 2-b, 2-c, 2-d, and 2-e are 3 wt % cationic PS 002 emulsion mixed with 1, 2, 3, 4, 5 wt% GO aqueous suspension. In the third row, 3-a, 3-b, 3-c, 3-d, and 3-e are 3 wt % cationic PS 010 emulsion mixed with 1, 2, 3, 4, 5 wt% GO aqueous suspension.

3.3. Electrostatic self-assembly

The results of electrostatic self-assembly after 240 min between cationic PS and GO with different content are shown in **Figure 5**. In the first row, the 1-a is the digital image of the cationic PS emulsion, and 1-b is pure PS emulsion mixed with GO aqueous suspension, which produces no sediment. The 1-c is the digital image of 3 wt% cationic PS 002 mixed with 1 wt% GO, and 1-d is 3 wt% cationic PS 010 mixed with 5 wt% GO. The 1-e is GO aqueous suspension. In the second row, 2-a, 2-b, 2-c, 2-d, and 2-e are 3 wt% cationic PS 002 emulsion mixed with 1, 2, 3, 4, 5 wt% GO aqueous suspension. In the third

row, 3-a, 3-b, 3-c, 3-d, and 3-e are 3 wt % cationic PS 010 emulsion mixed with 1, 2, 3, 4, 5 wt% GO aqueous suspension.

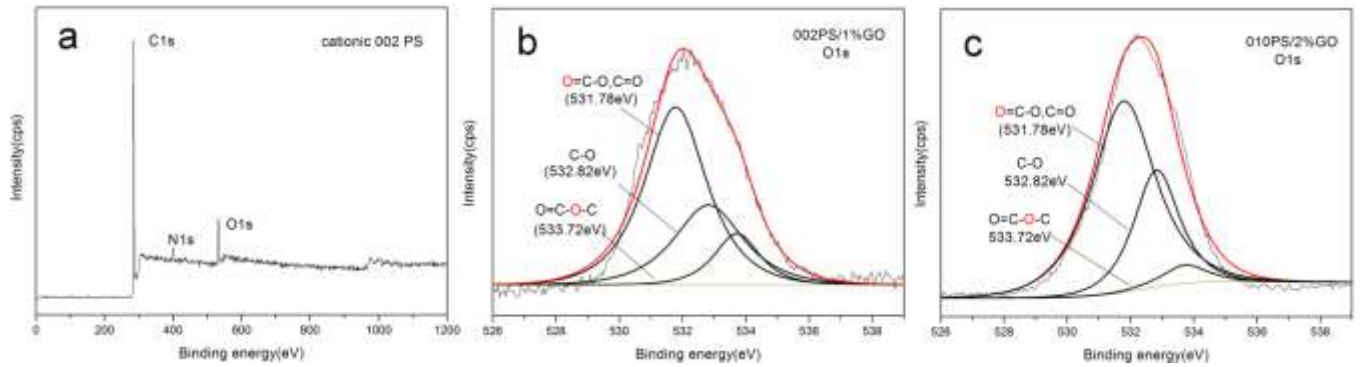

Fig.6 XPS spectra of PS/GO core-shell microspheres. **(a)** pure cationic PS 002. **(b)** O1s spectra of cationic PS 002 microspheres mixed with 1 wt% GO suspension. **(c)** O1s spectra of cationic PS 010 microspheres mixed with 2 wt% GO suspension.

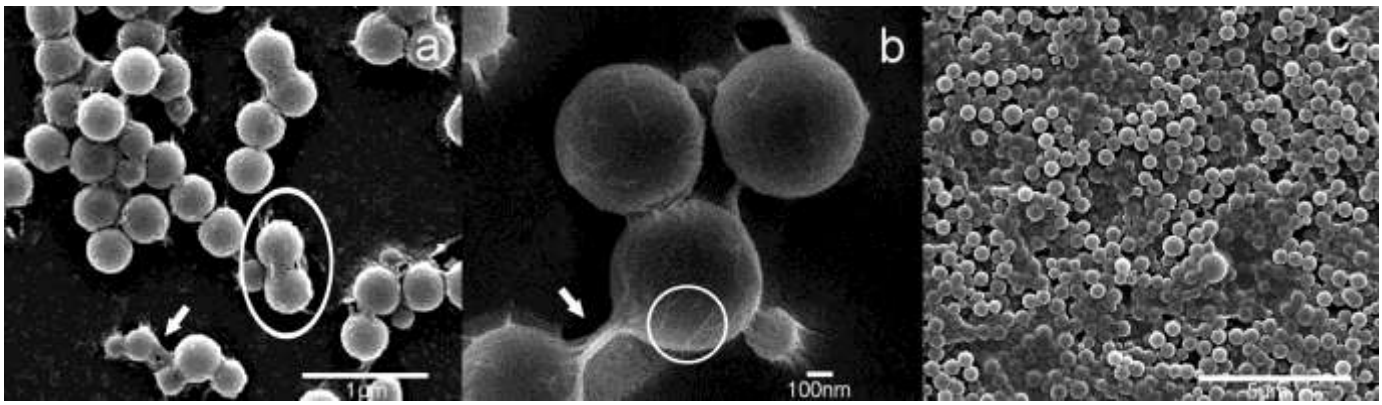

Fig.7 (a) and (b) PS/GO core-shell microspheres with different magnification (2-a in **Figure 5**). **(c)** pure PS microspheres mixed with GO 3 wt% GO suspension (1-b in **Figure 5**).

Table 1. Total element contents of each sample calculated according to the XPS spectra in **Figures 2, 4,** and **6**.

Sample	Total element contents		
	C	O	N
cationic PS 002	94.0%	3.1%	2.9%
cationic PS 010	93.5%	4.0%	2.5%
GO	69.9%	29.5%	0.6%
3 wt% cationic PS 002+1 wt% GO	90.8%	7.2%	2.0%
3 wt% cationic PS 010+2 wt% GO	90.1%	8.8%	1.1%

Table 1 shows the total element contents of each sample calculated according to the XPS spectra in **Figures 2, 4**, and **6**. Elements carbon, oxygen and nitrogen are contained in each sample. The total contents of element O in cationic PS 002 and cationic PS 010 are 3.1% and 4.00%. The total contents of element O in cationic PS 002 with GO and cationic PS 010 with GO are 7.2% and 8.8%. The increase of oxygen contents along with the decrease of nitrogen and carbon contents clearly demonstrates that GO has already overlaid onto the cationic PS microspheres. A careful study of nitrogen contents reveals more details. N content of PS 002 with GO coating is 2.0%, which is close to 2.9% of pure cationic PS 002. However, 1.1% of PS 010 with GO coating is closer to 0.6% of GO. This phenomenon indicates that cationic PS 010 mixed with GO generates a thicker core-shell structure. The thick shell of GO makes XPS not to be able to detect the interior structure**.** A detail analysis of O1s in **Figure 6** gives a similar result.

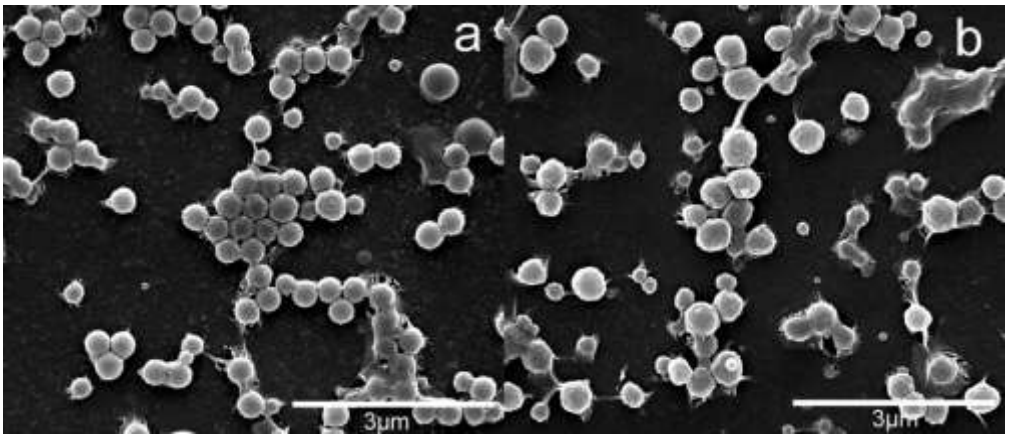

Fig. 8 SEM images of PS/GO core-shell microspheres. **(a)** from 3 wt% cationic PS 002 and 3 wt% GO aqueous suspension (2-c in **Figure 5**); **(b)** from 3 wt% cationic PS 010 and 3 wt% GO aqueous suspension (3-c in **Figure 5**).

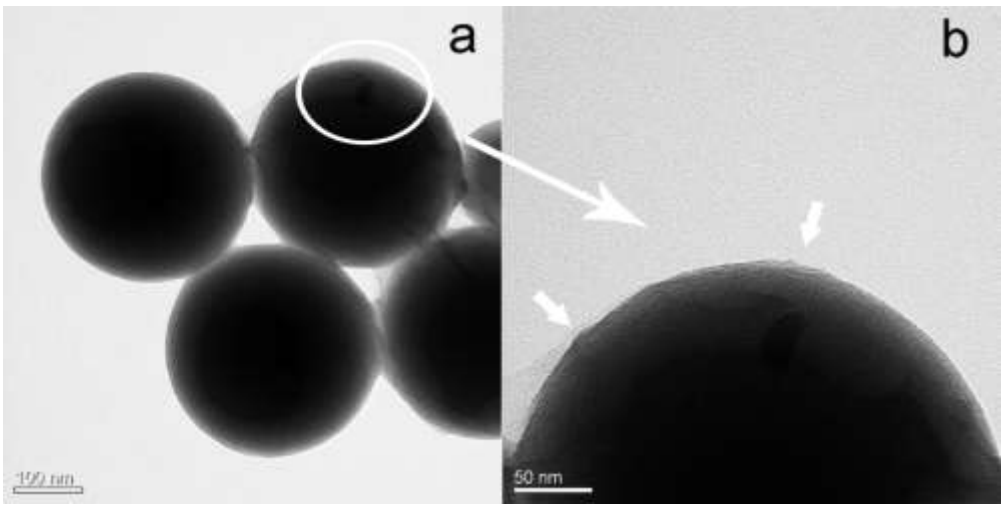

Fig. 9 TEM images of PS/GO core-shell microspheres assembly from cationic PS 002 and 1 wt% GO aqueous suspension with different magnification (2-a in **Figure 5**).

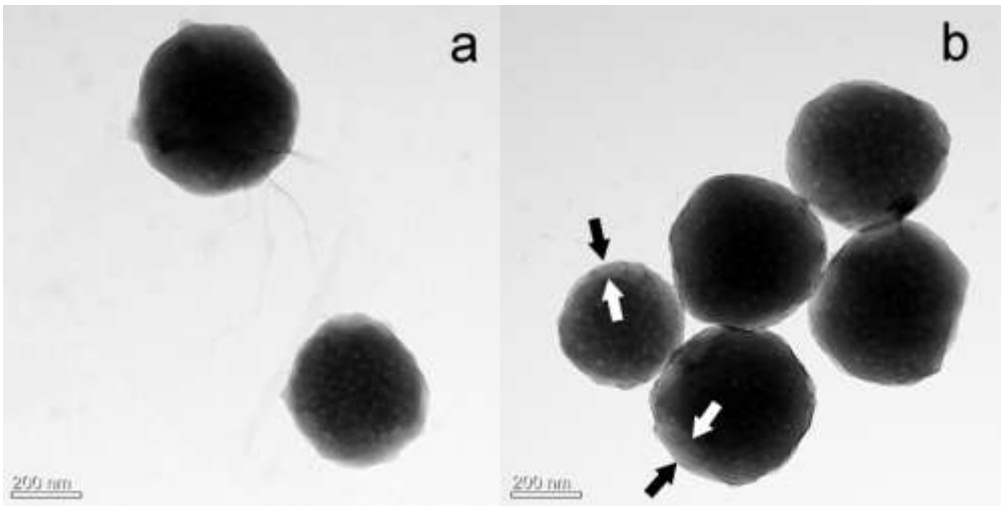

Fig. 10 TEM images of PS/GO core-shell microspheres which from 3 wt% cationic PS 010 and 3 wt% GO aqueous suspension (3-c in **Figure 5**).

In **Figure 5**, the images of the first row clearly illustrate that the specific electrostatic attraction only exists between the cationic PS and GO, other than other mixed systems. The second and the third rows show the results of electrostatic self-

assembly with different content of GO aqueous suspension from 1 wt% to 5 wt%. It can be observed that PS/GO assembly are quickly precipitated at the bottom of bottles in the case of 1 wt % GO with cationic PS 002 (2-a) and 3-5 wt % GO with cationic PS 010 (3-c, 3-d, 3-e), leaving transparent aqueous solution at the top of bottles. This also indicates that the used concentration of the cationic PS and GO nanosheets in 2-a, 3-c, 3-d, 3-e are exactly matched, which leads to the charge neutralization between the positive charge in the cationic PS and the negative charge in GO nanosheets, resulting in a fast precipitation. Actually, all the samples in the second and third rows of **Figure 5** produce a precipitation. However, except for 2-a, 3-c, 3-d, 3-e, other samples need 5-7 days. It is noted that both the PS emulsion and GO aqueous suspension are of near neutral pH in our study. The samples of 1-a, 1-b, 2-a, 2-c, and 3-c are chosen for further SEM and TEM analysis.

Figure 6 shows the O1s spectra of core-shell microspheres. **Figure 6(b)** is the O1s spectra of PS/GO core-shell microspheres assembled by 3 wt% cationic PS 002 and 1 wt% GO, and **Figure 6(c)** is the O1s spectra of core-shell microspheres generated from 3 wt% cationic PS 010 and 2 wt% GO. The peaks of 532.82 eV and 531.78 eV are the characteristic peaks of O=C−O, C=O and C−O in GO in **Figure 6(b)** and **6(c).**[43] The peak at 533.72 eV is assigned to O=C−O−C of cationic monomer DMC. It can be observed that the peak intensity at 533.72 eV of PS 010/GO core-shell microspheres is obviously weaker than that of PS 002/GO. The calculated the oxygen contents from O=C−O−C in **Figure 6(b)** and **Figure 6(c)** are 1.0% and 0.5%, respectively. This phenomenon is similar with the total oxygen contents listed in **Table 1**. The decrease of the oxygen content of O=C−O−C indicates a thicker GO layer in PS 010/GO microspheres, which agrees with the discussion for **Table 1**.

The morphology of the electrostatic assembly is observed by SEM, and shown in **Figure 7**. Clearly, PS/GO core-shell microspheres are formed via electrostatic assembly. **Figure 7(a)** and **7(b)** show the images of the typical core-shell microspheres assembly by 3 wt% cationic PS 002 and 1 wt% GO (2-a in **Figure 5**). **Figure 7(c)** is an SEM image with both smooth and wrinkled microspheres, which is just the simple mixture of pure PS emulsion and 3 wt% GO suspension (1-b in **Figure 5**). The GO nanosheets only cover parts of PS microspheres. It can be seen that all the polymer microspheres are successfully encapsulated by flexible and ultrathin GO nanosheets in **Figure 7(a)** and **7(b)**. In addition, rippled silk waves formed by redundant GO nanosheets can be clearly observed between each PS/GO core-shell microspheres, as marked by the arrow and the circle in **Figure 7(b)**. The reason behind this phenomenon is probably due to that GO nanosheets with a large area will not perfectly match with a single particle, resulting in the formation of the ribbon structure between microspheres.

Figure 8 shows the influence of the cationic PS with the different amount of cationic monomer on PS/GO core-shell microspheres. Both **Figure 8(a)** and **8(b)** show rippled silk waves on the surface of each microsphere. Compared to **Figure 8(a)**, the microspheres in **Figure 8(b)** have more attachments, presenting slightly deformation on the surface. This indicates a stronger electrostatic attraction force between cationic PS 010 microspheres and the negative charged GO nanosheets, and it leads to more GO covers and the deformation. Here the surface density of the positive charge plays a key role in controlling the surface morphology and core-shell structure of PS/GO microspheres.

TEM images of PS/GO core-shell microspheres assembly from cationic PS 002 and 1 wt% GO aqueous suspension (2-a in **Figure 5**) with different magnification are shown in **Figure 9.** It can be observed a nearly perfect core-shell microsphere with a layer of about 9-13 nm GO adsorbed tightly on the spherical surface, showing a clear outline of microspheres.

TEM images of the PS 010/GO core-shell microspheres (**Figure 10**) have obvious differences from the PS 002/GO core-shell microspheres (**Figure 9**) both in shape and the thickness of the shell structures. In **Figure 10**, the edge of core-shell microspheres in TEM images indicates that the GO nanosheets anchor tightly and thickly on the surface of cationic polymer microspheres, as marked in arrows. In addition, the margin of the core-shell microspheres in **Figure 10(a)** also shows the ribbon-like GO pieces, which are similar with the ribbon materials in SEM images. Particularly, in **Figure 10(b)**, from the edge of PS/GO core-shell microspheres, the thicknesses of the shell can be measured within 80-100nm, as indicated by arrows. Here, the thickness of the shell is uniform and much thicker compared to SiO_2/GO hybrids constructed through the hydrogen bonding between –NH_2 and –COOH.[34] In the present study, the method proposed achieves the 3D graphene oxide construction both in uniform thickness and strong binding force.

Figure 11(a), 11(b), and **11(c)** are the particle size distributions. Apparently, the particle size distribution of the pure PS and PS/GO core-shell microspheres from 3 wt% cationic PS 002 and 1 wt% GO (2-a in **Figure 5**) are mainly within the scope of 0.3-0.4 μm, and that of PS/GO core-shell microspheres from 3 wt% cationic PS 010 and 3 wt% GO (3-c in **Figure 5**) is within the scope of 0.4-0.5 μm along with a higher frequency in a larger size.

Figure 11(d) is XRD patterns of GO, cationic PS 002, and PS/GO core-shell microspheres from 3 wt% cationic PS 002 mixed with 1 wt% GO (2-a in **Figure 5**). All the samples in **Figure 11(d)** were dried into powders in a vacuum oven over night. A strong diffraction peak at $2\theta=10.59°$ is assigned to GO (001),[44] the corresponding d-spacing value of graphene oxide is calculated as $d_{(001)}=0.835$ nm based on Bragg equation ($\lambda=2d\sin\theta$), which is identical with the reported studies.[45-47] For the pattern of the cationic PS, the characteristic broad peak at around $2\theta=20.04°$ is obtained, which indicates the amorphous structure.[48] The pattern of PS/GO core-shell microspheres from 3 wt % cationic PS 002 and 1 wt % GO is similar to that of the cationic PS, and an only difference is the appearance of a weak peak at about

10.26°, which contributed from GO binding to the microspheres surface.[44]

4. Conclusions

In this study, a perfect 3D polymer/graphene oxide core-shell microspheres structure was successfully prepared via the electrostatic self-assembly. 2D graphene oxide nanosheets were successfully wrapped onto microspheres to form a 3D core-shell structure under the action of the electrostatic attraction force with a uniform thickness of the shell. The SEM and TEM images of rippled silk waves on the surface of PS/GO core-shell microspheres not only indicated the perfect polymer/GO core-shell structure, but also presented a strong binding between two materials. It was also revealed that the thickness of the shell of PS/GO core-shell microspheres was under good control and the thickness of the shell from different cationic PS microspheres (with 0.246% and 0.715% surface concentration of $-N(CH_3)_3^+$ groups) was 9-13 and 80-100 nm, respectively. We believe the method proposed here is a valuable tool for the controllable assembly of polymers and graphene oxide (or graphene). This method probably starts a new understanding on the interaction between graphene oxide and polymers.

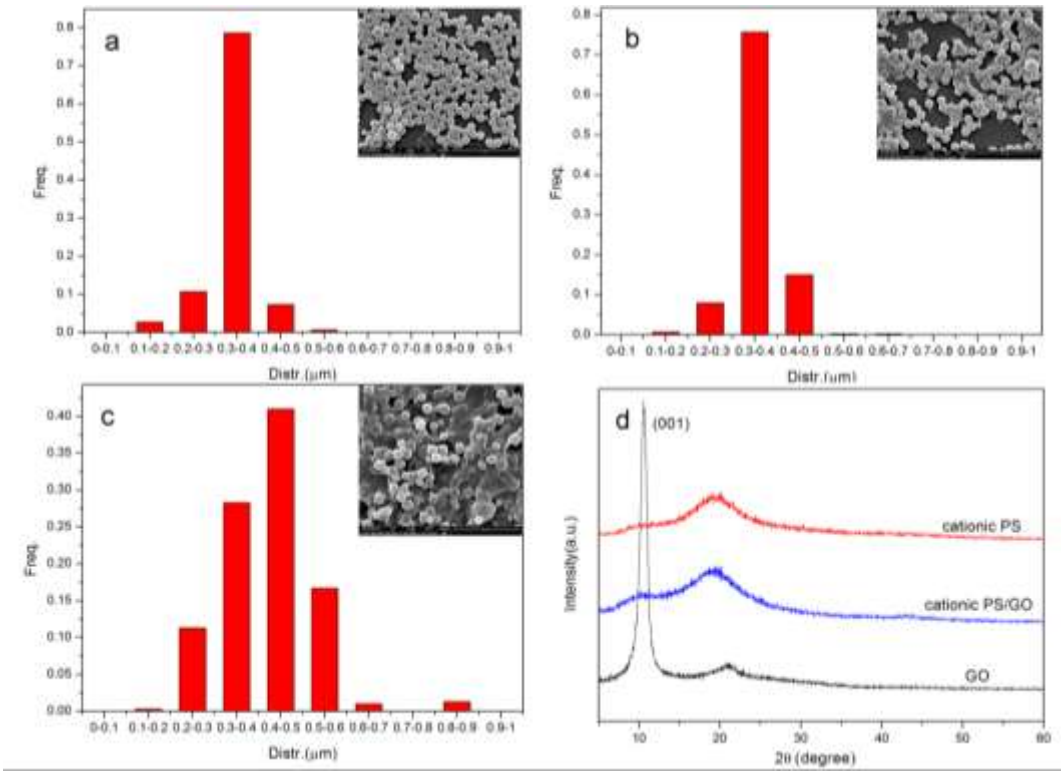

Fig. 11 Particle size distribution of PS/GO core-shell microspheres and XRD patterns. **(a)** powders of pure PS; **(b)** the PS/GO core-shell microspheres from 3 wt% cationic PS 002 and 1 wt% GO (2-a in **Figure 5**); **(c)** the PS/GO core-shell microspheres from 3 wt% cationic PS 010 and 3 wt% GO (3-c in **Figure 5**); **(d)** XRD patterns of GO, cationic PS 002, and PS/GO core-shell microspheres from 3 wt% cationic PS 002 and 1 wt% GO (2-a in **Figure 5**).

Acknowledgements

This work was supported by Research Center for Application of Graphene (Sichuan University-WuXi), State Key Laboratory of Polymer Materials Engineering (Grant No. sklpme2014-3-06), and the National Natural Science Foundation of China (Grant No. 51473104).

Notes and references

[a] State Key Laboratory of Polymer Materials Engineering of China, Polymer Research Institute, Sichuan University, Chengdu 610065, China

[b] Research Center for Application of Graphene (Sichuan University-WuXi), Wuxi, 214000, China

*Corresponding author. Tel.: +86-28-85402601; Fax: +86-28-85402465; E-mail address: jjbao2000@sina.com (J. Bao); zhoutaopoly@scu.edu.cn (T. Zhou)

1. X. Huang, X. Y. Qi, F. Boey, H. Zhang, *Chem. Soc. Rev.*, 2012, **41**, 666-686.
2. H. Bi, J. Chen, W. Zhao, S. R. Sun, *RSC Adv.*, 2013, **3**, 8454-8460.
3. A. Bhardwaj, A. K. Shukla, S. R. Dhakate, D. K. Misra, *RSC Adv.*, 2015, **5**, 11058-11070.
4. J. K. Lee, C. S. Park, H. Kim, *RSC Adv.*, 2014, **4**, 62453-62456.
5. Q. Peng, S. De, *RSC Adv.*, 2013, **3**, 24337-24344.
6. C. Y. Chang, S. P. Ju, J. W. Chang, S. C. Huang, H. W. Yang, *RSC Adv.*, 2014, **4**, 26074-26080.

7. A. Pandikumar, G. T. S. How, T. P. See, F. S. Omar, *et al.*, *RSC Adv.*, 2014, **4**, 63296-63323.
8. F. You, D. G. Wang, X. X. Li, M. J. Liu, *et al., RSC Adv.*, 2014, **4**, 8799-8807.
9. O. Jankovský, P. Šimek, D. Sedmidubský, *et al., RSC Adv.*, 2014, **4**, 7418-7424.
10. Y. Wang, Z. H. Li, J. Wang, J. H. Li, Y. H. Lin, *Tends in Biotechnol.*, 2011, **29**, 205-212.
11. N. Li, Z. P. Chen, W. C. Ren, F. Li, H. M. Cheng, *PNAS.*, 2012, **109**, 17360-17365.
12. Y. Gu, Y. Wang, *RSC Adv.*, 2014, **4**, 8582-8589.
13. Y. S. Luo, D. Z. Kong, Y. L. Jia, J. S. Luo, *et al., RSC Adv.*, 2013, **3**, 5851-5859.
14. R. Fang, X. P. Ge, M. Du, Z. Li, C. Z. Yang, *et al., Colloid Polym. Sci.*, 2014, **292**, 985-990.
15. G. H. Lee, R. C. Cooper, S. J. An, S. Lee, *et al., Science*, 2013, **340**, 1073-1076.
16. V. C. Tung, L. M. Chen, M. J. Allen, *et al., Nano. Lett.*, 2009, **9**, 1949-1955.
17. G. Eda, G. Fanchini, M. Chhowalla, *et al., Nat. Nanotech.*, 2008, **3**, 270-274.
18. X. W. Yang, L. Qiu, C. Cheng, *et al., Angew. Chem. Int. Ed.*, 2011, **50**, 7325-7328.
19. T. Sasaki, Y. Ebina, *et al., Chem. Commun.*, 2000, 2163-2164.
20. P. Podsiadlo, M. Michel, J. Lee, *et al., Nano Lett.*, 2008, **8**, 1762-1770.
21. L. J. Cote, F. Kim, J. X. Huang, *J. Am. Chem. Soc., 2*009, **131**, 1043-1049.
22. X. L. Li, G. Zhang, X. D. Bai, *et al., Nat. Nanotech.*, 2008, **3**, 538-542.
23. Y. X. Xu, K. X. Sheng, C. Li and G. Q. Shi, *ACS Nano*, 2010, **4**, 4324-4330.
24. F. Liu, T. S. Seo, *Adv. Funct. Mater.*, 2010, **20**, 1930-1936.
25. Z. J. Fan, J. Yan, L. J. Zhi, Q. Zhang, T. Wei, J. Feng, *et al., Adv. Mater.*, 2010, **22**, 3723-3728.
26. J. L. Vickery, A. J. Patil, S. Mann, *Adv. Mater.*, 2009, **21**, 2180-2184.
27. Z. H. Tang, S. L. Shen, J. Zhuang, X. Wang, *Angew. Chem. Int. Ed.*, 2010, **49**, 4603–4607.
28. X. Jiang, Y. Ma, J. Li, Q. Fan, W. Huang, *J. Phys. Chem. C*, 2010, **114**, 22462-22465.
29. H. L. Luo, G. Y. Xiong, Z. W. Yang, S. R. Raman, *et al., RSC Adv.*, 2014, **4**, 14369-14372.
30. X. C. Dong, Y. F. Cao, J. Wang, *et al., RSC Adv.*, 2012, **2**, 4364-4369.
31. Y. F. Zhang, M. Z. Ma, J. Yang, *et al., RSC Adv.*, 2014, **4**, 8466-8471.
32. P. F. Xie, X. P. Ge, B. Fang, Z. Li, *et al., Coll. Poly. Sci*., 2013, **291**, 1631-1639.
33. J. T. Yang, X. H. Yan, M. J. Wu, et al., *J. Nanopart Res.*, 2012, **14**, 717-725.
34. L. Huang, P. L. Zhu, G. Li, *et al., J. Mater. Chem. A*, 2014, **2**, 18246-18255.
35. S. Y. Li, T. Qian, S. S. Wu, J. Shen, *Chem. Commun*., 2012, **48**, 7997-7999.
36. W. S. Hummers, Jr., R. E. Offeman, *J. Am. Chem. Soc.*, 1958, **80**, 1339-1339.
37. S. Stankovich, D. A. Dikin, R. D. Piner, *et al., Carbon*, 2007, **45**, 1558-1565.
38. S. Chandra, S. Sahu, P. Pramanik, *Mater. Sci. Eng. B*, 2010, **167**, 133-136.
39. G. W. Zhang, W. Ao, C. Yang, J. Liu, J. J. Liu, *Petrochem. Technol*., 2011, **40**, 1057-1062.
40. X. Z. Kong, J. Lian, X. L. Zhu, X. L. Gu, Z. G. Zhang, *Acta Polym. Sinica*, 2008, **8**, 787-802.
41. M. Fossa, S. Diplasb, E. Gulbrandsenc, *Electrochimica Acta*, 2010, **55**, 4851-4857.
42. X. Mei, J. Y. Chen, N. Huang, *J. Funct. Mater.*, 2007, **38**, 1819-1821.
43. A. Bagri, C. Mattevi, M. Acik, Y. J. Chabal, *et al., Nat. Chem.*, 2010, **2**, 581-587.
44. Z. S. Zhao, Chao Zhang, et al., *J. Nanyang Normal Uni.*, 2010, **9**, 42-44.
45. G. X. Zhao, L. Jiang, Y.D. He, J. X. Li, *et al., Adv. Mater.*, 2011, **23**, 3959-3963.
46. M. Song, L. L. Yu, Y. M. Wu, *J. Nanomater.*, 2012, 135138-135143.
47. Y. H. Xue, Y. Liu, F. Lu, J. Qu, *et al., Phys. Chem. Lett.* 2012, **3**, 1607-1612.
48. Y. B. Zhao, J. F. Zhou, Z. J. Zhang, *Chem. Res.*, 1998, **9**, 16-19.

